



1 Trends and source apportionment of aerosols in Europe during
2 1980–2018

3

4

5 Yang Yang¹, Sijia Lou^{2*}, Hailong Wang³, Pinya Wang¹, Hong Liao¹

6

7

8

9 ¹Jiangsu Key Laboratory of Atmospheric Environment Monitoring and Pollution
10 Control, Jiangsu Collaborative Innovation Center of Atmospheric Environment and
11 Equipment Technology, School of Environmental Science and Engineering, Nanjing
12 University of Information Science and Technology, Nanjing, Jiangsu, China

13 ²School of Atmospheric Sciences, Nanjing University, Nanjing, Jiangsu, China

14 ³Atmospheric Sciences and Global Change Division, Pacific Northwest National
15 Laboratory, Richland, Washington, USA

16

17

18

19

20

21 *Correspondence to slou.nju@gmail.com



22 **Abstract**

23 Aerosols have significantly affected health, environment and climate in Europe.
24 Aerosol concentrations have been declining since 1980s in Europe, mainly owing to
25 the reduction of local aerosol and precursor emissions. Emissions from other source
26 regions of the world, which have been changing rapidly as well, may also perturb the
27 historical and future trends of aerosols and change their radiative impact in Europe.
28 This study examines trends of aerosols in Europe during 1980–2018 and quantify
29 contributions from sixteen source regions using the Community Atmosphere Model
30 version 5 with an Explicit Aerosol Source Tagging technique (CAM5-EAST). The
31 simulated near-surface total mass concentration of sulfate, black carbon and primary
32 organic carbon had a 62% decrease during 1980–2018, of which the majority was
33 contributed by reductions of local emissions in Europe and 8%-9% was induced by
34 the decrease in emissions from Russia-Belarus-Ukraine. With the decreases in the
35 fractional contribution of local emissions, aerosols transported from other source
36 regions are increasingly important to air quality in Europe. During 1980–2018, the
37 decrease in sulfate loading leads to a warming effect of 2.0 W m^{-2} in Europe, with
38 12% coming from changes in non-European sources, especially from North America
39 and Russia-Belarus-Ukraine. According to the Shared Socioeconomic Pathways
40 (SSP) scenarios, contributions to the sulfate radiative forcing over Europe from both
41 European local emissions and non-European emissions would decrease at a
42 comparable rate in the next three decades, suggesting that future changes in non-



43 European emissions are as important as European emissions in causing possible

44 regional climate change associated with aerosols in Europe.

45

46

47



48 **1. Introduction**

49 Aerosols are main air pollutants that contribute to excess morbidity and
50 premature mortality through damaging cardiovascular and respiratory systems
51 (Lelieveld et al., 2019). They also have adverse effects on atmospheric visibility for
52 road and air traffic (Vautard et al., 2009). During the 1952 London Fog, high fatality
53 associated with extremely high level of aerosols caused thousands of premature
54 deaths (Bell and Davis, 2001), which resulted in a number of air quality legislations
55 for reducing air pollution in Europe (Brimblecombe et al., 2006).

56 Besides the health and environment effects, aerosols can significantly impact
57 regional and global climate through perturbing the Earth's radiation fluxes and
58 influencing cloud microphysics (Boucher et al., 2013). Globally, anthropogenic
59 aerosols exert a net cooling effect in the Earth system, which have dampened the
60 warming driven by greenhouse gases since the pre-industrial era. Due to a strong
61 surface albedo feedback over polar regions, per unit aerosol emission from western
62 Europe was reported to have the greatest cooling effect than other major source
63 regions of the globe (Persad and Caldeira, 2018), revealing the importance of
64 understanding aerosol variations in Europe.

65 Significant reductions in near-surface aerosol concentrations and aerosol optical
66 depth (AOD) have been observed in Europe during the last few decades from long-
67 term station measurements and satellite retrievals (de Meij et al., 2012; Tørseth et
68 al., 2012). The decrease in aerosols has been considered as a cause of the increase
69 in surface solar radiation over Europe since the 1980s (Wild, 2009), as well as the



70 contributor of the eastern European warming (Vautard et al., 2009), Arctic
71 amplification (Acosta Navarro et al., 2016), and the increased atmospheric visibility
72 over Europe (Stjern et al., 2011) during the past three decades.

73 The decrease in aerosols over Europe was mainly attributed to the continuous
74 reductions in European local anthropogenic emissions of aerosols and precursor
75 gases since the 1980s (Smith et al., 2011), as a result of legislations for improving
76 air quality. In addition to local emissions, aerosol levels can also be affected by
77 aerosol transport at continental scales (Zhang et al., 2017; Yang et al., 2018a).
78 Aerosol emissions in major economic regions of the world have been changing
79 rapidly during the past few decades owing to economic development and
80 environmental measures. North America has started reducing emissions since the
81 1980s, and emissions in Russia also showed decreasing trends after the dissolution
82 of the Soviet Union (Smith et al., 2011). In the meantime, aerosol emissions from
83 East Asia and South Asia have largely increased due to economic growth, although
84 emissions in China have been undergoing a remarkable reduction in the most recent
85 years, as a result of strict air quality regulations (Streets et al., 2000; Li et al., 2017).
86 It is important to understand the relative roles of local emissions and regional
87 transport in affecting long-term variation of aerosols in Europe from both air quality
88 and climate perspectives.

89 Source apportionment is useful for quantifying contributions to aerosols from
90 specific source regions and/or sectors, which is beneficial to the emission control
91 strategies. The traditional method of examining the source-receptor relationship in



92 aerosol models is to zero out or perturb a certain percent of emissions from a given
93 source region or sector in parallel sensitivity simulations along with a baseline
94 simulation, which has been used in many studies to examine source contributions of
95 particulate matter (PM) in Europe from different sectors (e.g., Sartelet et al., 2012;
96 Tagaris et al., 2015; Aksoyoglu et al., 2016). Recently, source region contributions to
97 European CO and O₃ levels, as well as global and regional aerosol radiative forcing,
98 were examined under the Hemispheric Transport of Air Pollution model experiment
99 phase 2 (HTAP2) protocol, in which sensitivity simulations were conducted with
100 anthropogenic emissions from different source regions reduced by 20% (Jonson et
101 al., 2018). This method suffers a large computational cost for the excessive model
102 simulations when estimating contributions from a large number of sources, and
103 contributions from all sources do not sum up to 100% of the total concentration in the
104 default simulation (Koo et al., 2009; Wang et al., 2014).

105 The explicit aerosol tagging method, which simultaneously tracks contributions
106 from many different sources, is a useful tool for assessing source-receptor
107 relationship of aerosols. This method has previously been adopted in regional air
108 quality models such as CAMx (the Comprehensive Air quality Model with
109 Extensions) and CMAQ (the Community Multi-scale Air Quality model). Using
110 regional air quality models with aerosol tagging, contributions from different source
111 sectors and local/regional sources to European PM and its health impact were
112 studied (Brandt et al., 2013; Skylakou et al., 2014; Karamchandani et al., 2017).
113 However, due to the limitation in domain size of regional air quality models,



114 contributions of intercontinental transport from sources outside the domain are
115 difficult to be accounted.

116 Anthropogenic emissions of aerosols and their precursor gases from different
117 economic regions of the world have changed substantially during the past few
118 decades. Very few studies have examined the source apportionment of aerosols in
119 Europe from sources all over the changing world. In this study, source attributions of
120 concentrations, column burden, optical depth of aerosols in four major areas of
121 Europe from sixteen source regions of the globe over 1980–2018 are quantified,
122 which is facilitated by the explicit aerosol source tagging technique that were recently
123 implemented in a global aerosol-climate model (CAM5-EAST). This technique has
124 lately been used to examine source attribution of aerosol trends in China and U.S.
125 during 1980–2014 (Yang et al., 2018a,b). The source apportionment analysis is
126 extended to year 2018 using the Shared Socioeconomic Pathways (SSPs) scenario,
127 with a focus on Europe here.

128 The CAM5-EAST model, along with the aerosol source tagging technique, and
129 aerosol emissions are described in Sect. 2. Section 3 evaluates the model
130 performance in simulating aerosols in Europe. Section 4 show the analysis of
131 source-receptor relationships of aerosols in Europe in climatological mean. Source
132 contributions to long-term variations of European aerosols and their direct radiative
133 forcing (DRF) during 1980–2018, as well as future forcing prediction, are provided in
134 Sect. 5. Section 6 summarizes these results and conclusions.

135 **2. Methods**



136 **2.1 Model Description and Experimental Setup**

137 The global aerosol-climate model CAM5 (Community Atmosphere Model version
138 5), which was developed as the atmospheric component of CESM (the Community
139 Earth System Model, Hurrell et al., 2013), is applied to simulate aerosols at a spatial
140 resolution of 1.9° latitude × 2.5° longitude and 30 vertical layers from the surface to
141 3.6 hPa. Aerosol species, including sulfate, black carbon (BC), primary organic
142 aerosol (POA), second organic aerosol (SOA), mineral dust and sea salt, can be
143 simulated in a modal aerosol module of CAM5. The three-mode aerosol module
144 (MAM3) configuration is chosen with the consideration of the computational
145 efficiency of long-term simulation. Details of the MAM3 aerosol representation in
146 CAM5 are described in Liu et al. (2012). On top of the default CAM5, some aerosol-
147 related scheme modifications are utilized to improve the model performance in the
148 aerosol convective transport and wet deposition (Wang et al., 2013).

149 A 40-year (1979–2018) historical AMIP-type (Atmospheric Model
150 Intercomparison Project) simulation has been performed, following CMIP6 (the
151 Coupled Model Intercomparison Project Phase 6) configurations and forcing
152 conditions. Time-varying sea surface temperatures, sea ice concentrations, solar
153 insolation, greenhouse gas concentrations and aerosol emissions are prescribed in
154 the simulation. To better reproduce large-scale circulation patterns for aerosol
155 transport in the model, wind fields are nudged to the MERRA-2 (Modern Era
156 Retrospective-Analysis for Research and Applications Version 2) reanalysis (Ronald
157 Gelaro et al., 2017).



158 Aerosol DRF is defined in this study as the difference in clear-sky radiative fluxes
159 at the top of the atmosphere between two parallel calculations in the radiative
160 transfer scheme with and without specific aerosols accounted, respectively.
161 Historical variation of aerosol DRF due to anthropogenic emissions from Europe and
162 outside Europe are quantified in this study. Future DRF of sulfate aerosol over
163 Europe is also estimated through scaling historical mean (1980–2018) sulfate DRF
164 by the ratio of SSPs future SO₂ emissions to historical emissions assuming a linear
165 response of DRF to AOD and regional emissions. This DRF prediction method has
166 been used to estimate the East Asian contribution to sulfate DRF in U.S. in 2030s
167 (Yang et al., 2018a).

168 **2.2 Aerosol Source Tagging Technique**

169 The Explicit Aerosol Source Tagging (EAST) technique, which was recently
170 implemented in CAM5 (Wang et al., 2014; Yang et al., 2017a, b), is used to examine
171 the long-term source apportionment of aerosols in Europe. Unlike the traditional
172 back-trajectory and emission perturbation methods, EAST has the identical physical,
173 chemical and dynamical processes considered independently for aerosol species
174 (defined as new tracers) emitted from each of the tagged source region and/or sector
175 in the simulation. Sulfate, BC, POA and SOA from pre-defined sources can be
176 explicitly tracked, from emission to deposition, in one CAM5-EAST simulation. Due
177 to the computational constraint and potentially large model bias from the simplified
178 SOA treatment (Yang et al., 2018a; Lou et al., 2019), we focus on sulfate, BC and
179 POA in this study but quantify the potential impact of SOA on the aerosol variation.



180 The global aerosol and precursor emissions are decomposed into sixteen source
181 regions defined in the HTAP2 protocol, including Europe (EUR), North America
182 (NAM), Central America (CAM), South America (SAM), North Africa (NAF), South
183 Africa (SAF), the Middle East (MDE), Southeast Asia (SEA), Central Asia (CAS),
184 South Asia (SAS), East Asia (EAS), Russia-Belarus-Ukraine (RBU), Pacific-
185 Australia-New Zealand (PAN), the Arctic (ARC), Antarctic (ANT), and Non-
186 Arctic/Antarctic Ocean (OCN) (Figure 1). Note that sources from marine and volcanic
187 eruptions are included in OCN. The focused receptor region in this study is Europe,
188 which is further divided into Northwestern Europe (NWE or NW Europe),
189 Southwestern Europe (SWE or SW Europe), Eastern Europe (EAE or E. Europe)
190 and Greece-Turkey-Cyprus (GTC) based on the finer source region selection in
191 HTAP2.

192 **2.3 Aerosol and Precursor Emissions**

193 Following the CMIP6-AMIP protocol, historical anthropogenic (Hoesly et al.,
194 2018) and biomass burning (van Marle et al., 2017) emissions of aerosol and
195 precursor gases are used over 1979–2014. For the remaining four years (2015–
196 2018), emissions are interpolated from the SSP2-4.5 forcing scenario, in which
197 aerosol pathways are not as extreme as other SSPs and have been used in many
198 model intercomparison projects for CMIP6 (O'Neill et al., 2016). Figure 2 shows the
199 spatial distribution and time series of anthropogenic emissions of SO₂ (precursor gas
200 of sulfate aerosol), BC and POA from Europe over 1980–2018. High emissions are
201 located over E. Europe and NW Europe, from which the emissions of SO₂, BC and



202 POA were reduced by 84–93%, 43–62% and 28–36%, respectively, in 2014–2018
203 relative to 1980–1984. Although SW Europe had a relatively low total amount of
204 emissions compared to E. Europe and NW Europe, it had significant reductions in
205 SO₂ and BC emissions, 91% and 55%, respectively. Over GTC region, SO₂ and BC
206 emissions were increased by 49% and 48%, respectively. Considering the sub-
207 regions as a whole, SO₂, BC and POA emissions from Europe have decreased by
208 12.57 Tg yr⁻¹ (83%), 0.22 Tg yr⁻¹ (46%) and 0.30 Tg yr⁻¹ (24%) in 2014–2018
209 compared to 1980–1984 (Table 1). Historical changes in emissions from other
210 source regions can be found in Hoesly et al. (2018) and Yang et al. (2018b).

211 **3 Model Evaluation**

212 Compared to the observational data from EMEP (European Monitoring and
213 Evaluation Programme, <http://www.emep.int>) networks during 2010–2014, CAM5-
214 EAST can well reproduce the spatial distribution and magnitude of aerosol
215 components with normalized mean biases (NMB) of -14%~23% and correlation
216 coefficients (R) in a range of 0.43~0.62 for sulfate, BC and organic carbon (OC,
217 derived from POA and SOA from the model results) (Figures 3a, b, c). The model
218 underestimates the mean concentration of PM_{2.5} (sum of sulfate, BC, POA and SOA)
219 by 59% relative to EMEP data (Figure 3d), although the spatial distribution has a
220 strong correlation with the observations (R=0.72). It is partially because the model
221 version used in this study does not have the ability to simulate nitrate and
222 ammonium aerosols, which can be the major constituents of PM_{2.5} in some regions,



223 and the fine-mode mineral dust and sea salt is not included in the estimated $PM_{2.5}$
224 either.

225 Figure 4 shows the time series of annual mean near-surface sulfate, BC, OC and
226 $PM_{2.5}$ concentrations averaged over EMEP sites in Europe and the corresponding
227 model values during 1993–2018. Variations in near-surface sulfate and $PM_{2.5}$
228 concentrations are consistent between the model and observations, with R values
229 higher than 0.9. $PM_{2.5}$ concentrations are lower in the model simulation than
230 observations in almost all years, confirming the role of the missing aerosol species in
231 contributing to $PM_{2.5}$ as discussed above. The observed variations of BC and OC
232 concentrations in Europe are represented in the simulation, with R values of 0.52
233 and 0.65, respectively. However, the observed high values of BC and OC
234 concentrations are not captured by the model, probably because very few data were
235 available before 2010 and, therefore, any difference between model and observation
236 cannot be smoothed out through the spatial average. This is also indicated by the
237 large spatial variation of BC and OC concentrations before 2010. Nevertheless, the
238 modeled concentrations are still within the range of observations. Note that the
239 number of sites used for the spatial average in Figure 4 is different from year to year
240 and thus the variation or trend here does not represent that over a sub-region or the
241 entire Europe.

242 The modeled AOD is evaluated against the AERONET (Aerosol Robotic
243 Network, <https://aeronet.gsfc.nasa.gov>) data in Figure 8. Both the modeled and
244 observed AOD show decreasing trends during 2001–2018. The model



245 underestimates AOD in all four sub-regions of Europe probably due to the lack of
246 nitrate and ammonium aerosols. The variations of AOD in Western Europe
247 (combined NW and SW Europe) are well predicted with R values of about 0.75, but
248 the model barely reproduces the AOD variations in E. Europe and the GTC region
249 ($R < 0.5$). The difference of the interannual variation in AOD between the model
250 simulation and observation can be caused by many factors such as aerosol
251 emissions, aerosol parameterizations in model, aerosol mixing state, inaccurate
252 meteorological fields from reanalysis data, and biases in measurements. However,
253 identifying the contribution of each factor to the difference is beyond the scope of this
254 paper.

255 **4. Source Apportionment of Aerosols in Europe**

256 Based on the tagging technique in CAM5-EAST, near-surface concentrations of
257 total sulfate-BC-POA can be attributed to emissions within and outside Europe, as
258 shown in Figures 5a and 5b, and the relative contributions in percentage are given in
259 Figures 5c and 5d. Averaged over 2010–2018, due to the relatively high local
260 emissions, annual mean sulfate-BC-POA concentrations contributed by European
261 emissions show peak values of $4 \mu\text{g m}^{-3}$ in E. Europe. The slight increase in SO_2
262 emission from the GTC region (Figure 2), which is opposite to the decreases in the
263 other three sub-regions of Europe, also leads to high concentrations in GTC, with 2–
264 $4 \mu\text{g m}^{-3}$ contributed by European emissions. Due to the atmospheric transport from
265 surrounding regions including North Africa, the Middle East and RBU, non-European
266 emissions account for $0.5\text{--}1 \mu\text{g m}^{-3}$ over SW Europe, E. Europe and GTC area.



267 Overall, European local emissions are the dominant sources of sulfate-BC-POA
268 near-surface concentrations in Europe with contributions larger than 80% (60%) in
269 central areas (most of Europe). Non-European emissions are responsible for 30–
270 50% of the near-surface concentrations near the coastal areas and boundaries of the
271 Europe that are easily influenced by aerosol regional transport.

272 Figure 6 illustrates the source contributions in percentage of emissions from
273 different regions of the globe to near-surface aerosol concentrations and column
274 burdens over the four sub-regions of Europe averaged over 2010–2018. Different
275 aerosols have fairly different local/remote source attributions depending on the local
276 to remote emission ratio and transport efficiency. European emissions explain 54%–
277 68% of near-surface sulfate concentrations over the four sub-regions of Europe, with
278 the largest local contribution from E. Europe due to the relatively high emission rate.
279 The emissions from Europe dominate BC and POA concentrations in Europe with
280 contributions in the range of 78%–95% and 58%–78%, respectively. The impact of
281 local emissions on near-surface sulfate concentration is smaller than BC and POA.
282 This is partially due to the less efficient gas scavenging than particles and the
283 additional SO₂-to-sulfate conversion process that increases the atmospheric
284 residence time of sulfur. On the other hand, the higher initial injection height of SO₂
285 emissions from some sources (e.g., industrial sector and power plants) facilitates the
286 lifting of SO₂ and sulfate aerosol into the free atmosphere and, therefore, favors the
287 long-range transport (Yang et al., 2019). The efficient reduction in local SO₂



288 emissions in Europe also caused the lower influences of local emissions on sulfate
289 concentrations in recent years.

290 Anthropogenic emissions over oceans (e.g., international shipping) and natural
291 emissions of oceanic dimethyl sulfide (DMS) and volcanic activities together account
292 for 16%–28% of near-surface sulfate concentrations in the four sub-regions of
293 Europe. About 10% of sulfate and 5%–10% of BC and POA in E. Europe and GTC
294 come from RBU emissions. North Africa contributes to 7% of sulfate, 17% of BC and
295 24% of POA over SW Europe. The contributions of emissions, from the Middle East,
296 to aerosol concentrations in GTC are between 5% and 10%.

297 The transboundary and intercontinental transport of aerosols occur most
298 frequently in the free troposphere rather than near the surface, leading to larger
299 relative contributions from non-European sources to aerosol column burdens than to
300 the near-surface concentrations (Figure 6). The European emissions only contribute
301 32%–47% of column burden of sulfate, 57%–75% of BC and 51%–71% of POA over
302 the four sub-regions of Europe. Over NW Europe and SW Europe, about 10%–15%
303 of the sulfate burden is from East Asia and RBU, respectively. Sources in North
304 Africa are responsible for 27% and 14% of BC and 19% and 11% of POA burden
305 over SW Europe and GTC, respectively. Emissions from North America account for
306 15% and 10% POA burden over NW Europe and SW Europe, respectively.
307 Emissions from RBU explain 12% and 19% of POA burden over E. Europe and
308 GTC, respectively. Since near-surface aerosol concentrations directly affect air
309 quality and column burden is more relevant to radiative impact, the differences of



310 relative contributions between near-surface concentrations and column burden
311 highlight the possible roles of non-local emissions in either air quality or energy
312 balance over Europe.

313 **5. Source Apportionment of Long-term Trends**

314 Total sulfate-BC-POA concentrations decreased during 1980–2018 over all of
315 the four sub-regions of Europe (Figure 7), since that near-surface aerosol
316 concentrations in Europe are dominated by its local emissions and the European
317 anthropogenic emissions have significantly decreased during this time period.
318 Averaged over the entire Europe, near-surface concentrations of sulfate, BC and
319 POA decreased by 70%, 43% and 23%, respectively, between 1980–1984 and
320 2014–2018, which is consistent with the decreases in local emissions (Table 1). The
321 total sulfate-BC-POA concentrations decreased by 62%. With SOA included, this
322 value does not have a substantial change (from 62% to 59%) and the decreasing
323 trends in the four sub-regions of the Europe are not largely affected either. The
324 column burden of sulfate, BC, POA and the sum of these three decreased by 60%,
325 28%, 4% and 55%, respectively, which is less than the decrease in corresponding
326 near-surface concentration. It is because non-local emissions have larger influences
327 at high altitudes than at the surface, which partly dampened the contribution of near-
328 surface aerosol decrease (induced by reductions in local emissions) to the
329 column integration.

330 The decrease in European local emissions explains 93% of the reduced
331 concentration and 91% of the reduced burden in Europe between the first and last



332 five-year period of 1980–2018, while 8%–9% is contributed by the reduction in
333 emissions from RBU (Table 2). The decrease in emissions from North America also
334 explains 10% of the reduced column burden of sulfate-BC-POA in Europe from
335 1980–1984 to 2014–2018. Along with the decreases in local emission contributions
336 to near-surface sulfate-BC-POA concentrations in Europe, the fraction of non-
337 European emission contributions increased from 10%–30% to 30%–50% during
338 1980–2018 (Figure 7), indicating that aerosols from foreign emissions through long-
339 range transport have become increasingly important to air quality in Europe.
340 Regulations for further improvement of air quality in Europe in the near future need
341 to take changes in non-European emissions into account.

342 Similar to the declining trend in column burden, simulated total AOD also
343 decreased from 0.12–0.16 to 0.06–0.08 in NW Europe and SW Europe and from
344 0.19–0.21 to 0.09–0.13 in E. Europe and GTC region during the past four decades
345 (Figure 8). Sulfate AOD accounts for the largest portion of total combustion AOD
346 (sum of sulfate, BC, POA and SOA) over the four sub-regions of Europe. The
347 combustion AOD has decreased by 0.065 from 1980–1984 to 2014–2018 (Table 1),
348 with 0.059 (91%) contributed by the decrease in sulfate AOD. Therefore, we focus
349 on sulfate aerosol when examining the decadal changes in AOD and DRF in Europe
350 below.

351 The decreased sulfate AOD can also be decomposed into different contributions
352 from individual source regions in CAM5-EAST. European local emissions contribute
353 to 89% of the decrease, followed by 9% and 7% attributed to changes in emissions



354 from RBU and North America, respectively, with the residual offset by other source
355 regions (Table 2). Over the last four decades, model simulated sulfate AOD
356 decreased at a rate of 0.017, 0.017, 0.026 and 0.012 decade⁻¹, respectively, over
357 NW Europe, SW Europe, E. Europe and GTC. Decreases in European local SO₂
358 emissions result in 78% of the sulfate AOD decreases over GTC and about 90%
359 over the other three sub-regions (Figure 9). For the remote sources, emission
360 changes in North America explain 5%–10% of the European sulfate AOD decrease,
361 while RBU sources contribute 29% of the sulfate AOD decrease over GTC and 6%–
362 8% over NW Europe and E. Europe, indicating a possible warming enhancement
363 effect of changes in emissions from North America and RBU.

364 Averaged over 1980–2018, sulfate imposed a cooling effect over Europe with the
365 maximum negative DRF at the top of the atmosphere (TOA) exceeding -3 W m^{-2} in
366 E. Europe (Figure 10). Compared to 1980–1984, the magnitude of sulfate DRF
367 decreased in 2014–2018, leading to a $1\text{--}3 \text{ W m}^{-2}$ warming mainly in E. Europe. The
368 warming effect mostly came from local SO₂ emission reduction, while non-European
369 emission changes only contributed less than 0.4 W m^{-2} over most regions of the
370 Europe. Considering Europe as a whole, the decrease in sulfate DRF caused a
371 warming effect of 2.0 W m^{-2} , with 88% and 12% coming from reductions European
372 local emissions and changes in non-European emissions, respectively (Tables 1 and
373 2).

374 Future changes in sulfate DRF associated with European and non-European
375 emissions based on eight SSP scenarios are also estimated and shown in Figure 11.



376 Sulfate DRF contributed by both European and non-European emissions would
377 decrease in the near future but has large variabilities between different SSPs. The
378 sulfate DRF (cooling) over Europe contributed from European local emissions shows
379 a decrease from -0.48 W m^{-2} in year 2015 to -0.18 ($-0.08 \sim -0.33$) W m^{-2} in year 2030
380 and -0.14 ($-0.05 \sim -0.29$) W m^{-2} in year 2050. Unlike their contributions to the
381 historical (1980–2018) change, non-European emissions have an increasingly
382 significant impact on the future sulfate DRF changes in Europe. The contributions of
383 non-European emissions decrease from -0.68 W m^{-2} in year 2015 to -0.39 ($-0.13 \sim -$
384 0.64) W m^{-2} in year 2030 and -0.26 ($-0.08 \sim -0.63$) W m^{-2} in year 2050, with the
385 changes in a magnitude similar to that of European local emissions. It suggests that
386 future changes in non-European emissions are as important as European emissions
387 to radiative balance and associated regional climate change in Europe.

388 **6. Conclusions**

389 Using a global aerosol-climate model with an explicit aerosol source tagging
390 technique (CAM5-EAST), we examine the long-term trends and source
391 apportionment of aerosols in Europe over 1980–2018 from sixteen source regions
392 covering the globe in this study. CAM5-EAST can well capture the spatial distribution
393 and temporal variation of aerosol species in Europe during this time period, although
394 it underestimates $\text{PM}_{2.5}$ concentration and total AOD due in part to the lack of
395 representation of nitrate and ammonium aerosols in the model.

396 Averaged over 2010–2018, European emissions account for 54%–68%, 78%–
397 95% and 58%–78% of near-surface sulfate, BC, and POA concentrations over



398 Europe, respectively. RBU emissions explain 10% of sulfate in E. Europe and GTC.
399 North Africa contributes to 17% of BC and 24% of POA over SW Europe.
400 Anthropogenic emissions over oceans (e.g., from international shipping) and natural
401 emissions from marine and volcanic activities together account for 16%–28% of
402 sulfate near-surface concentrations in Europe. European emissions only account for
403 32%–47%, 57%–75% and 51%–71% of column burden of sulfate, BC and POA,
404 respectively, in Europe, with the rest contributed by emissions from East Asia, RBU,
405 North Africa and North America.

406 Compared to 1980–1984, simulated total sulfate-BC-POA near-surface
407 concentration and column burden over 2014–2018 had a decrease of 62% and 55%,
408 respectively, the majority of which was contributed by reductions in European local
409 emissions. The decrease in emissions from RBU contributed 8%–9% of the near-
410 surface concentration decrease, while the decrease in emissions from North America
411 accounted for 10% of the reduced column burden. With the large decrease in local
412 emission contribution, aerosols from foreign sources became increasingly important
413 to air quality in Europe. The decrease in sulfate led to a 2.0 W m^{-2} warming in
414 Europe, with 12% coming from changes in non-European emissions, especially in
415 North America and RBU. Based on the SSP scenarios and the assumed relationship
416 between DRF and emissions, we estimated that sulfate DRF over Europe
417 contributed from European emissions and non-European emissions would decrease
418 at a comparable rate in the near future. This suggests that future changes in non-
419 European emissions are as important as European emissions in affecting regional



420 climate change associated with aerosols in Europe. It should also be noted that the
421 model currently does not have the ability to simulate nitrate and ammonium aerosols
422 and, therefore, the conclusions may not hold with all aerosols.
423
424



425 ***Data availability.***

426 The default CAM5 model is publicly available at
427 <http://www.cesm.ucar.edu/models/cesm1.2/> (last access: 16 August 2019). Our
428 CAM5-EAST model code and results can be made available through the National
429 Energy Research Scientific Computing Center (NERSC) servers upon request.

430

431 ***Competing interests.***

432 The authors declare that they have no conflict of interest.

433

434 ***Author contribution.***

435 YY, SL, and HW designed the research; YY performed the model simulations; YY,
436 and SL analyzed the data. All the authors discussed the results and wrote the paper.

437

438 ***Acknowledgments.***

439 This research was supported by the National Natural Science Foundation of China
440 under grant 41975159, the U.S. Department of Energy (DOE), Office of Science,
441 Biological and Environmental Research as part of the Earth and Environmental
442 System Modeling program, Jiangsu Specially Appointed Professor Project, and the
443 Startup Fund for Talent at NUIST under Grant 2019r047. The Pacific Northwest
444 National Laboratory is operated for DOE by Battelle Memorial Institute under
445 contract DE-AC05-76RLO1830. The National Energy Research Scientific Computing
446 Center (NERSC) provided computational support.



447 **References**

448

449 Acosta Navarro, J. C., Varma, V., Riipinen, I., Seland, Ø., Kirkevåg, A., Struthers,
450 Iversen, H., T., Hansson, H.-C., and Ekman, A. M. L.: Amplification of Arctic
451 warming by past air pollution reductions in Europe, *Nat. Geosci.*, 9, 277–281,
452 <https://doi.org/10.1038/ngeo2673>, 2016.

453

454 Aksoyoglu, S., Baltensperger, U., and Prévôt, A. S. H.: Contribution of ship
455 emissions to the concentration and deposition of air pollutants in Europe, *Atmos.*
456 *Chem. Phys.*, 16, 1895–1906, doi:10.5194/acp-16-1895-2016, 2016.

457

458 Bell, M. L., and Davis, D. L.: Reassessment of the Lethal London Fog of 1952: Novel
459 Indicators of Acute and Chronic Consequences of Acute Exposure to Air
460 Pollution, *Environ. Health Perspect.*, 109, 389–394,
461 <https://doi.org/10.1289/ehp.01109s3389>, 2001.

462

463 Boucher, O., Randall, D., Artaxo, P., Bretherton, C., Feingold, G., Forster, P.,
464 Kerminen, V. M., Kondo, Y., Liao, H., Lohmann, U., Rasch, P., Satheesh, S. K.,
465 Sherwood, S., Stevens, B., and Zhang, X. Y.: Clouds and Aerosols, in: *Climate*
466 *Change 2013: The Physical Science Basis, Contribution of Working Group I to*
467 *the Fifth Assessment Report of the Intergovernmental Panel on Climate Change*,
468 edited by: Stocker, T. F., Qin, D., Plattner, G.-K., Tignor, M., Allen, S. K.,
469 Boschung, J., Nauels, A., Xia, Y., Bex, V., Midgley, P. M. Cambridge University
470 Press, Cambridge, United Kingdom and New York, NY, USA, 571–658, 2013.

471

472 Brandt, J., Silver, J. D., Christensen, J. H., Andersen, M. S., Bønløkke, J. H.,
473 Sigsgaard, T., Geels, C., Gross, A., Hansen, A. B., Hansen, K. M., Hedegaard,
474 G. B., Kaas, E., and Frohn, L. M.: Contribution from the ten major emission
475 sectors in Europe and Denmark to the health-cost externalities of air pollution
476 using the EVA model system – an integrated modelling approach, *Atmos. Chem.*
477 *Phys.*, 13, 7725–7746, <https://doi.org/10.5194/acp-13-7725-2013>, 2013.

478

479 Brimblecombe, P.: The Clean Air Act after 50 Years, *Weather*, 61, 311–314,
480 <https://doi.org/10.1256/wea.127.06>, 2006.

481

482 de Meij, A., Pozzer, A., and Lelieveld, J.: Trend analysis in aerosol optical depths
483 and pollutant emission estimates between 2000 and 2009, *Atmos. Environ.*, 51,
484 75–85, <https://doi.org/10.1016/j.atmosenv.2012.01.059>, 2012.

485

486 Gelaro, R., McCarty, W., Suárez, M. J., Todling, R., Molod, A., Takacs, L., Randles,
487 C. A., Darmenov, A., Bosilovich, M. G., Reichle, R., Wargan, K., Coy, L.,
488 Cullather, R., Draper, C., Akella, S., Buchard, V., Conaty, A., da Silva, A. M., Gu,
489 W., Kim, G.-K., Koster, R., Lucchesi, R., Merkova, D., Nielsen, J. E., Partyka, G.,
490 Pawson, S., Putman, W., Rienecker, M., Schubert, S. D., Sienkiewicz, M., and



- 491 Zhao, B.: The Modern-Era Retrospective Analysis for Research and
492 Applications, Version 2 (MERRA-2), *J. Climate*, 30, 5419–5454,
493 <https://doi.org/10.1175/JCLI-D-16-0758.1>, 2017.
494
- 495 Hoesly, R. M., Smith, S. J., Feng, L., Klimont, Z., Janssens-Maenhout, G., Pitkanen,
496 T., Seibert, J. J., Vu, L., Andres, R. J., Bolt, R. M., Bond, T. C., Dawidowski, L.,
497 Kholod, N., Kurokawa, J.-I., Li, M., Liu, L., Lu, Z., Moura, M. C. P., O'Rourke, P.
498 R., and Zhang, Q.: Historical (1750–2014) anthropogenic emissions of reactive
499 gases and aerosols from the Community Emissions Data System (CEDS),
500 *Geosci. Model Dev.*, 11, 369–408, <https://doi.org/10.5194/gmd-11-369-2018>,
501 2018.
502
- 503 Hurrell, J. W., Holland, M. M., Gent, P. R., Ghan, S., Kay, J. E., Kushner, P. J.,
504 Lamarque, J. F., Large, W. G., Lawrence, D., Lindsay, K., Lipscomb, W. H.,
505 Long, M. C., Mahowald, N., Marsh, D. R., Neale, R. B., Rasch, P., Vavrus, S.,
506 Vertenstein, M., Bader, D., Collins, W. D., Hack, J. J., Kiehl, J., and Marshall, S.:
507 The Community Earth System Model A Framework for Collaborative Research,
508 *B. Am. Meteorol. Soc.*, 94, 1339–1360, <https://doi.org/10.1175/BAMS-D-12-00121.1>, 2013.
509
- 510
- 511 Jonson, J. E., Schulz, M., Emmons, L., Flemming, J., Henze, D., Sudo, K., Tronstad
512 Lund, M., Lin, M., Benedictow, A., Koffi, B., Dentener, F., Keating, T., Kivi, R.,
513 and Davila, Y.: The effects of intercontinental emission sources on European air
514 pollution levels, *Atmos. Chem. Phys.*, 18, 13655–13672,
515 <https://doi.org/10.5194/acp-18-13655-2018>, 2018.
516
- 517 Karamchandani, P., Long, Y., Pirovano, G., Balzarini, A., and Yarwood, G.: Source-
518 sector contributions to European ozone and fine PM in 2010 using AQMEII
519 modeling data, *Atmos. Chem. Phys.*, 17, 5643–5664, <https://doi.org/10.5194/acp-17-5643-2017>, 2017.
520
- 521
- 522 Koo, B., Wilson, G. M., Morris, R. E., Dunker, A. M., and Yarwood, G.: Comparison
523 of source apportionment and sensitivity analysis in a particulate matter air quality
524 model, *Environ. Sci. Technol.*, 43, 6669–6675,
525 <https://doi.org/10.1021/es9008129>, 2009.
526
- 527 Lelieveld, J., Klingmüller, K., Pozzer, A., Burnett, R. T., Haines, A. and Ramanathan,
528 V.: Effects of fossil fuel and total anthropogenic emission removal on public
529 health and climate, *Proc. Natl. Acad. Sci.*, 116, 7192–7197,
530 <https://doi.org/10.1073/pnas.1819989116>, 2019.
531
- 532 Li, C., McLinden, C., Fioletov, V., Krotkov, N., Carn, S., Joiner, J., Streets, D., He,
533 H., Ren, X., Li, Z., and Dickerson, R. R.: India Is Overtaking China as the



- 534 World's Largest Emitter of Anthropogenic Sulfur Dioxide, *Scientific Reports*, 7,
535 14304, <https://doi.org/10.1038/s41598-017-14639-8>, 2017.
536
- 537 O'Neill, B. C., Tebaldi, C., van Vuuren, D. P., Eyring, V., Friedlingstein, P., Hurtt, G.,
538 Knutti, R., Kriegler, E., Lamarque, J.-F., Lowe, J., Meehl, G. A., Moss, R., Riahi,
539 K., and Sanderson, B. M.: The Scenario Model Intercomparison Project
540 (ScenarioMIP) for CMIP6, *Geosci. Model Dev.*, 9, 3461–3482,
541 <https://doi.org/10.5194/gmd-9-3461-2016>, 2016.
542
- 543 Persad, G. G., and Caldeira, K.: Divergent global - scale temperature effects from
544 identical aerosols emitted in different regions, *Nat. Commun.*, 9, 3289.
545 <https://doi.org/10.1038/s41467-018-05838-6>, 2018.
546
- 547 Riahi, K., van Vuuren, D. P., Kriegler, E., Edmonds, J., O'Neill, B. C., Fujimori, S.,
548 Bauer, N., Calvin, K., Dellink, R., Fricko, O., Lutz, W., Popp, A., Crespo
549 Cuaresma, J., KC, S., Leimbach, M., Jiang, L., Kram, T., Rao, S., Emmerling, J.,
550 Ebi, K., Hasegawa, T., Havlik, P., Humpenöder, F., Aleluia Da Silva, L., Smith,
551 S., Stehfest, E., Bosetti, V., Eom, J., Gernaat, D., Ma-sui, T., Rogelj, J., Strefler,
552 J., Drouet, L., Krey, V., Luderer, G., Harmsen, M., Takahashi, K., Baumstark, L.,
553 Doelman, J., Kainuma, M., Klimont, Z., Marangoni, G., Lotze-Campen, H.,
554 Obersteiner, M., Tabeau, A., and Tavoni, M.: The Shared Socioeconomic
555 Pathways and their energy, land use, and greenhouse gas emissions
556 implications: An Overview, *Global Environ. Chang.*, 42, 153–168,
557 <https://doi.org/10.1016/j.gloenvcha.2016.05.009>, 2017.
558
- 559 Sartelet, K. N., Couvidat, F., Seigneur, C., and Roustan, Y.: Impact of biogenic
560 emissions on air quality over Europe and North America, *Atmos. Environ.*, 53,
561 131–141, <https://doi.org/10.1016/j.atmosenv.2011.10.046>, 2012.
562
- 563 Skylakou, K., Murphy, B. N., Megaritis, A. G., Fountoukis, C., and Pandis, S. N.:
564 Contributions of local and regional sources to fine PM in the megacity of Paris,
565 *Atmos. Chem. Phys.*, 14, 2343–2352, [https://doi.org/10.5194/acp-14-2343-](https://doi.org/10.5194/acp-14-2343-2014)
566 2014, 2014.
567
- 568 Smith, S. J., van Aardenne, J., Klimont, Z., Andres, R. J., Volke, A., and Delgado
569 Arias, S.: Anthropogenic sulfur dioxide emissions: 1850–2005, *Atmos. Chem.*
570 *Phys.*, 11, 1101–1116, <https://doi.org/10.5194/acp-11-1101-2011>, 2011.
571
- 572 Stjern, C. W., Samset, B. H., Myhre, G., Bian, H., Chin, M., Davila, Y., Dentener, F.,
573 Emmons, L., Flemming, J., Haslerud, A. S., Henze, D., Jonson, J. E., Kucsera,
574 T., Lund, M. T., Schulz, M., Sudo, K., Takemura, T., and Tilmes, S.: Global and
575 regional radiative forcing from 20 % reductions in BC, OC and SO₄ – an HTAP2
576 multi-model study, *Atmos. Chem. Phys.*, 16, 13579–13599,
577 <https://doi.org/10.5194/acp-16-13579-2016>, 2016.



- 578
579 Stjern, C. W., Stohl, A., and Kristjánsson, J. E.: Have aerosols affected trends in
580 visibility and precipitation in Europe?, *J. Geophys. Res.*, 116, D02212,
581 <https://doi.org/10.1029/2010JD014603>, 2011.
582
- 583 Streets, D. G., Tsai, N. Y., Akimoto, H., and Oka, K.: Sulfur dioxide emissions in Asia
584 in the period 1985–1997, *Atmos. Environ.*, 34, 4413–4424,
585 [https://doi.org/10.1016/S1352-2310\(00\)00187-4](https://doi.org/10.1016/S1352-2310(00)00187-4), 2000.
586
- 587 Tagaris, E., Sotiropoulou, R., Gounaris, N., Andronopoulos, S., and Vlachogiannis,
588 D.: Effect of the Standard Nomenclature for Air Pollution (SNAP) categories on
589 air quality over Europe, *Atmosphere*, 6, 1119, doi:10.3390/atmos6081119, 2015.
590
- 591 Tørseth, K., Aas, W., Breivik, K., Fjæraa, A. M., Fiebig, M., Hjellbrekke, A. G., Lund
592 Myhre, C., Solberg, S., and Yttri, K. E.: Introduction to the European Monitoring
593 and Evaluation Programme (EMEP) and observed atmospheric composition
594 change during 1972–2009, *Atmos. Chem. Phys.*, 12, 5447–5481,
595 <https://doi.org/10.5194/acp-12-5447-2012>, 2012.
596
- 597 van Marle, M. J. E., Kloster, S., Magi, B. I., Marlon, J. R., Daniau, A.-L., Field, R. D.,
598 Arneeth, A., Forrest, M., Hantson, S., Kehrwald, N. M., Knorr, W., Lasslop, G., Li,
599 F., Mangeon, S., Yue, C., Kaiser, J. W., and van der Werf, G. R.: Historic global
600 biomass burning emissions for CMIP6 (BB4CMIP) based on merging satellite
601 observations with proxies and fire models (1750–2015), *Geosci. Model Dev.*, 10,
602 3329–3357, <https://doi.org/10.5194/gmd-10-3329-2017>, 2017.
603
- 604 Vautard, R., Yiou, P., and Oldenborgh, G.: Decline of fog, mist and haze in Europe
605 over the past 30 years, *Nat. Geosci.*, 2, 115–119,
606 <https://doi.org/10.1038/ngeo414>, 2009.
607
- 608 Wang, H., Easter, R. C., Rasch, P. J., Wang, M., Liu, X., Ghan, S. J., Qian, Y., Yoon,
609 J.-H., Ma, P.-L., and Vinoj, V.: Sensitivity of remote aerosol distributions to
610 representation of cloud–aerosol interactions in a global climate model, *Geosci.*
611 *Model Dev.*, 6, 765–782, <https://doi.org/10.5194/gmd-6-765-2013>, 2013.
612
- 613 Wang, H., Rasch, P. J., Easter, R. C., Singh, B., Zhang, R., Ma, P.-L., Qian, Y.,
614 Ghan, S. J., and Beagley, N.: Using an explicit emission tagging method in
615 global modeling of source–receptor relationships for black carbon in the Arctic:
616 Variations, sources, and transport pathways, *J. Geophys. Res.-Atmos.*, 119,
617 12888–12909, <https://doi.org/10.1002/2014JD022297>, 2014.
618
- 619 Wild, M.: Global dimming and brightening: A review, *J. Geophys. Res.*, 114,
620 D00D16, <https://doi.org/10.1029/2008JD011470>, 2009.
621



- 622 Yang, Y., Wang, H., Smith, S. J., Ma, P.-L., and Rasch, P. J.: Source attribution of
623 black carbon and its direct radiative forcing in China, *Atmos. Chem. Phys.*, 17,
624 4319–4336, <https://doi.org/10.5194/acp-17-4319-2017>, 2017a.
625
- 626 Yang, Y., Wang, H., Smith, S. J., Easter, R., Ma, P.-L., Qian, Y., Yu, H., Li, C., and
627 Rasch, P. J.: Global source attribution of sulfate concentration and direct and
628 indirect radiative forcing, *Atmos. Chem. Phys.*, 17, 8903–8922,
629 <https://doi.org/10.5194/acp-17-8903-2017>, 2017b.
630
- 631 Yang, Y., Wang, H., Smith, S. J., Zhang, R., Lou, S., Yu, H., Li, C., and Rasch, P. J.:
632 Source apportionments of aerosols and their direct radiative forcing and long-
633 term trends over continental United States, *Earth's Future*, 6, 793–808,
634 <https://doi.org/10.1029/2018EF000859>, 2018a.
635
- 636 Yang, Y., Wang, H., Smith, S. J., Zhang, R., Lou, S., Qian, Y., Ma, P.-L., and Rasch,
637 P. J.: Recent intensification of winter haze in China linked to foreign emissions
638 and meteorology, *Sci. Rep.*, 8, 2107, [https://doi.org/10.1038/s41598-018-20437-](https://doi.org/10.1038/s41598-018-20437-7)
639 7, 2018b.
640
- 641 Yang, Y., Smith, S. J., Wang, H., Lou, S., and Rasch, P. J.: Impact of anthropogenic
642 emission injection height uncertainty on global sulfur dioxide and aerosol
643 distribution, *J. Geophys. Res.-Atmos.*, 124, 4812–4826.
644 <https://doi.org/10.1029/2018JD030001>, 2019.
645
- 646 Zhang, Q., Jiang, X., Tong, D., Davis, S. J., Zhao, H., Geng, G., Feng, T., Zheng, B.,
647 Lu, Z., Streets, D. G., Ni, R., Brauer, M., van Donkelaar, A., Martin, R. V., Huo,
648 H., Liu, Z., Pan, D., Kan, H., Yan, Y., Lin, J., He, K., and Guan, D.:
649 Transboundary health impacts of transported global air pollution and
650 international trade, *Nature*, 543, 705–709, <https://doi.org/10.1038/nature21712>,
651 2017.
652
653
654



655 **Table 1.** Annual emissions (Tg yr^{-1}), concentrations ($\mu\text{g m}^{-3}$), column burden (mg m^{-2})
 656 2), AOD (scaled up by a factor of 100) and DRF (W m^{-2}) of Sulfate, BC, POA, SBP
 657 (sulfate-BC-POA) and $\text{PM}_{2.5}$ (sulfate-BC-POA-SOA) in Europe averaged over 1980–
 658 1984 and 2014–2018, as well as the differences between 1980–1984 and 2014–
 659 2018. Differences in percentage relative to mean values in 1980–1984 are presented
 660 in parentheses.
 661

		Emis.	Conc.	Burden	AOD*100	DRF
Sulfate	1980–1984	15.10	6.00	14.35	9.13	-3.27
	2014–2018	2.53	1.80	5.79	3.24	-1.24
	Δ	-12.57 (-83.2)	-4.20 (-70.0)	-8.55 (-59.6)	-5.89 (-64.6)	2.04 (-62.2)
BC	1980–1984	0.47	0.4	0.38	0.7	--
	2014–2018	0.25	0.23	0.28	0.5	--
	Δ	-0.22 (-45.8)	-0.17 (-43.0)	-0.11 (-27.6)	-0.21 (-29.2)	--
POA	1980–1984	1.24	1.12	1.12	0.63	--
	2014–2018	0.94	0.86	1.08	0.58	--
	Δ	-0.30 (-24.4)	-0.26 (-23.2)	-0.04 (-3.8)	-0.05 (-7.5)	--
Sulfate-BC-POA	1980–1984	--	7.52	15.85	10.46	--
	2014–2018	--	2.89	7.15	4.32	--
	Δ	--	-4.63 (-61.6)	-8.70 (-54.9)	-6.15 (-58.7)	--
$\text{PM}_{2.5}$	1980–1984	--	10.48	19.58	11.92	--
	2014–2018	--	4.34	8.55	5.44	--
	Δ	--	-6.14 (-58.6)	-11.03 (-56.3)	-6.48 (-54.37)	--

662
 663

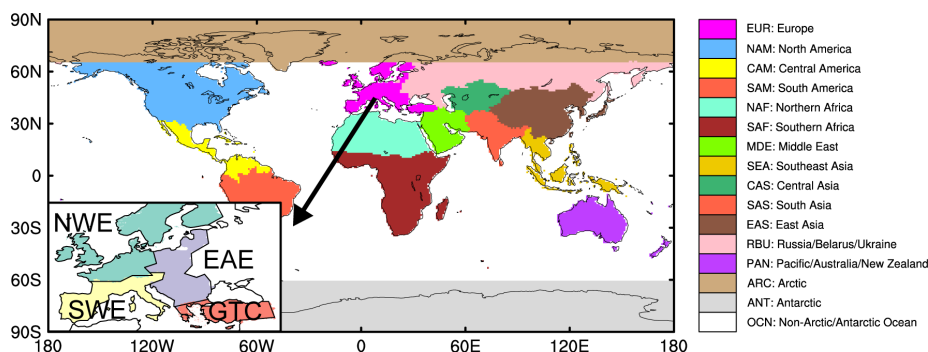


664 **Table 2.** Relative contributions (%) of emissions from major source regions to the
 665 changes in near-surface concentrations, column burden, AOD and DRF in Europe
 666 between 1980–1984 and 2014–2018.
 667

	Sulfate-BC- POA		
	Δ Conc.	Δ Burden	Δ AOD
EUR	92.8	91.2	91.2
NAM	1.8	10.0	6.5
NAF	-1.0	-1.5	-1.6
MDE	-0.9	-1.9	-1.5
EAS	-0.3	-3.1	-1.7
RBU	8.0	9.2	8.5
OTH	-0.1	-4.2	-2.0
OCN	-0.3	0.2	0.6

	Sulfate			
	Δ Conc.	Δ Burden	Δ AOD	Δ DRF
EUR	91.3	89.2	88.9	88.2
NAM	2.1	10.5	6.9	
NAF	-0.6	-0.9	-0.8	
MDE	-0.8	-1.7	-1.3	
EAS	-0.3	-2.8	-1.4	11.8
RBU	8.6	9.5	8.7	
OTH	-0.1	-4.0	-1.8	
OCN	-0.3	0.3	0.7	

668
 669
 670

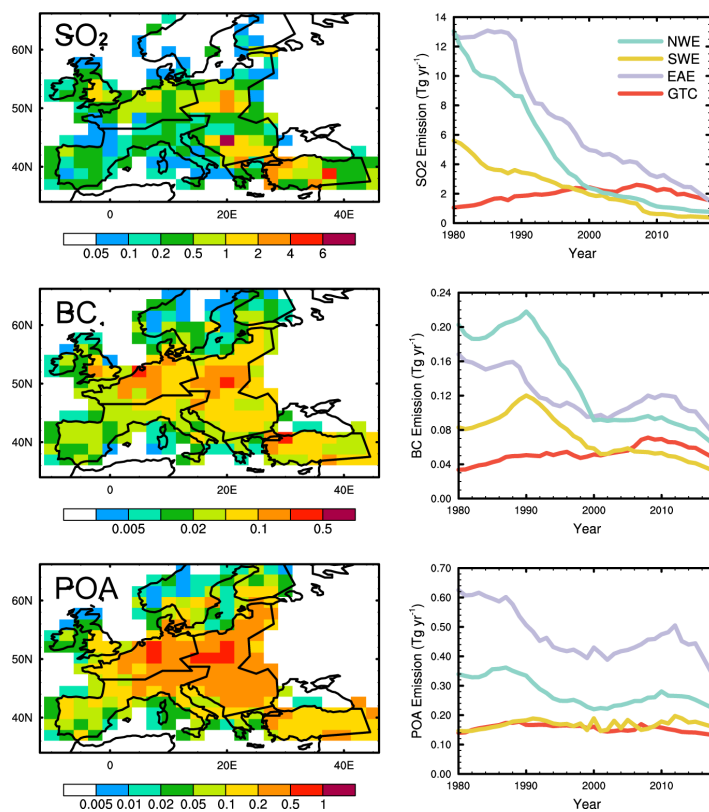


671

672

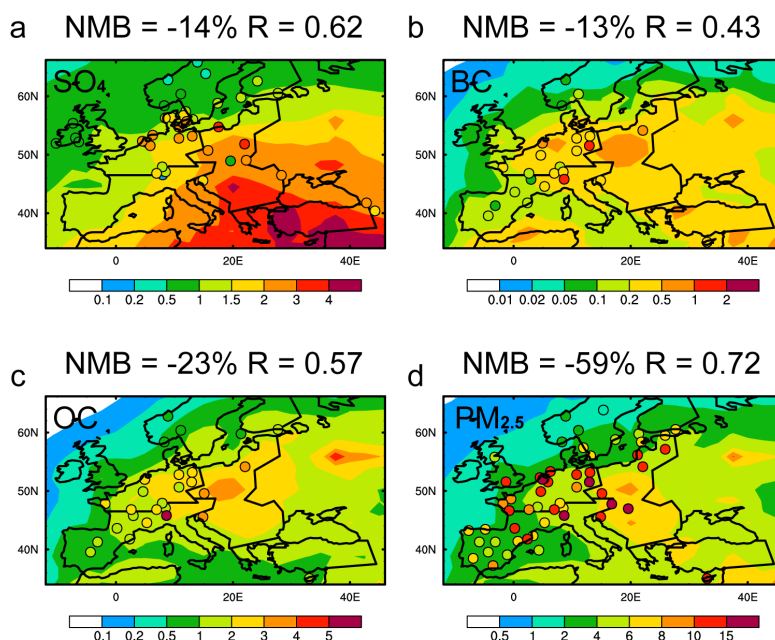
673 **Figure 1.** Source regions that are selected for the Explicit Aerosol Source Tagging
674 (EAST) in this study, including Europe (EUR), North America (NAM), Central
675 America (CAM), South America (SAM), North Africa (NAF), South Africa (SAF), the
676 Middle East (MDE), Southeast Asia (SEA), Central Asia (CAS), South Asia (SAS),
677 East Asia (EAS), Russia-Belarus-Ukraine (RBU), Pacific-Australia-New Zealand
678 (PAN), the Arctic (ARC), Antarctic (ANT), and Non-Arctic/Antarctic Ocean (OCN).
679 The embedded panel (at bottom left) is Europe, as the receptor region, which is
680 further divided to Northwestern Europe (NWE), Southwestern Europe (SWE),
681 Eastern Europe (EAE) and Greece-Turkey-Cyprus (GTC).

682



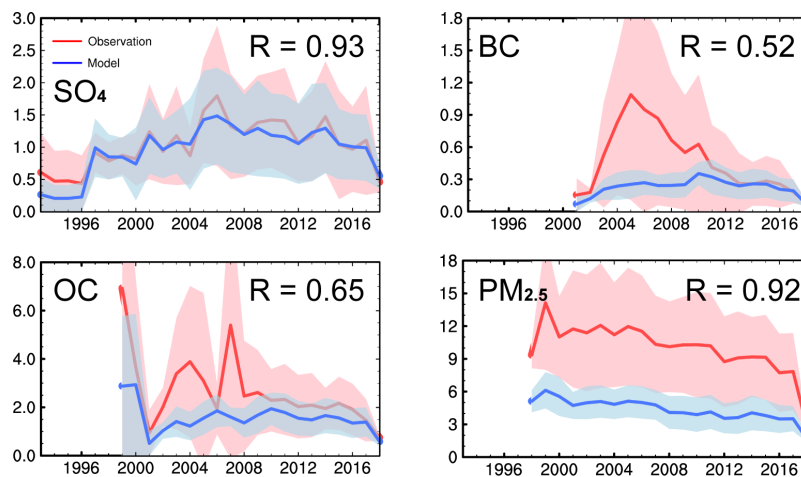
683
684
685
686
687
688
689
690

Figure 2. Spatial distribution (left) of annual mean (1980–2018) SO₂ (top), BC (middle) and POA (bottom) emissions (Tg m⁻² yr⁻¹) over Europe. Time series (1980–2018) of annual total SO₂, BC and POA emissions (Tg yr⁻¹) from the four sub-regions of Europe.



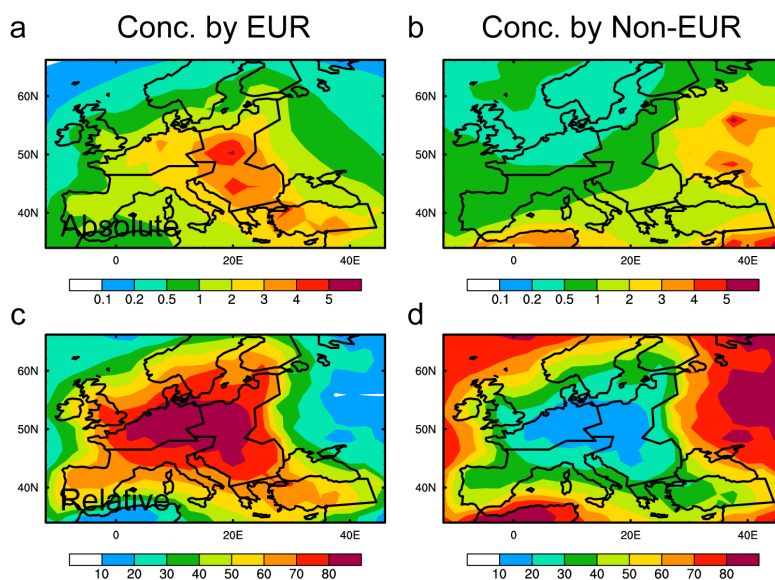
691
692
693
694
695
696
697
698
699
700

Figure 3. Spatial distribution of simulated (contour) and observed (color-filled circles) annual mean near-surface (a) sulfate, (b) BC, (c) OC (derived as (POA+SOA)/1.4 in model) and (d) PM_{2.5} (sulfate+BC+POA+SOA in model) concentrations ($\mu\text{g m}^{-3}$) over 2010–2014. Observations are from EMEP (European Monitoring and Evaluation Programme) networks. Normalized mean bias ($\text{NMB} = 100\% \times \frac{\sum(\text{Model}_{\text{site}} - \text{Observation}_{\text{site}})}{\sum \text{Observation}_{\text{site}}}$) and correlation coefficient (R) between observed and simulated concentrations are noted at the top of each panel.



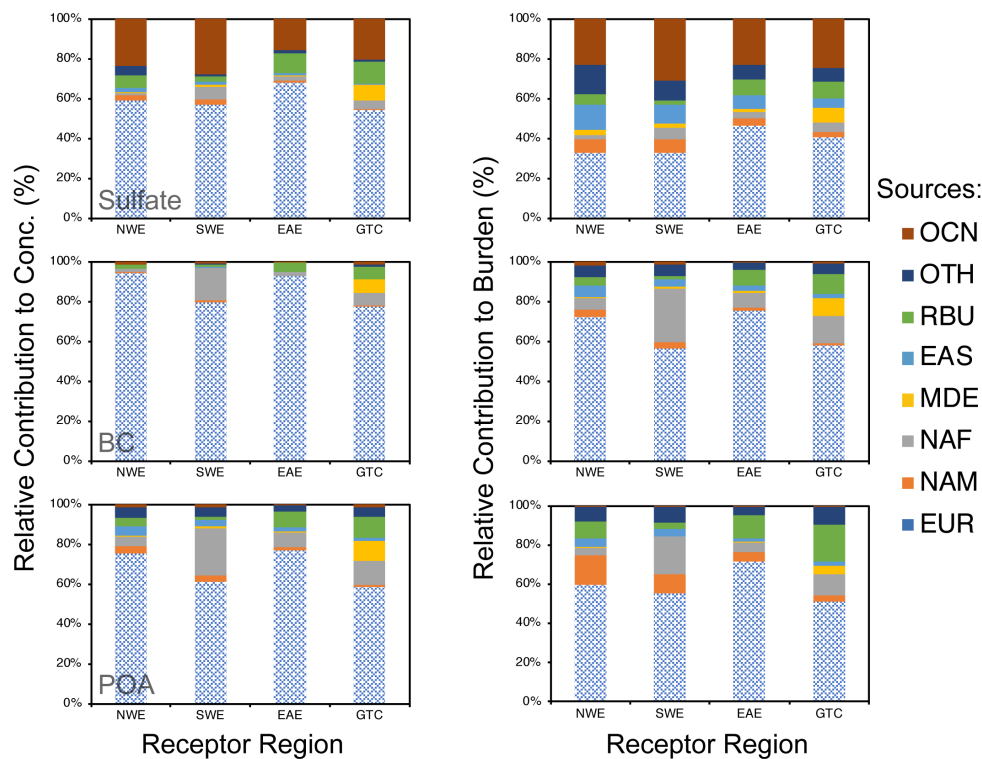
701
702
703
704
705
706
707
708
709
710
711

Figure 4. Time series (1993–2018) of spatial and annual mean near-surface sulfate, BC, OC and PM_{2.5} concentrations ($\mu\text{g m}^{-3}$) in Europe from model simulation (blue lines) and observations (red lines). Model results are plotted only when EMEP observational data are available. Shaded areas represent 1- σ spatial standard deviation of annual mean concentrations for each year. Temporal correlation coefficients (R) between observed and simulated spatially averaged concentrations are noted on the top-right corner of each panel.



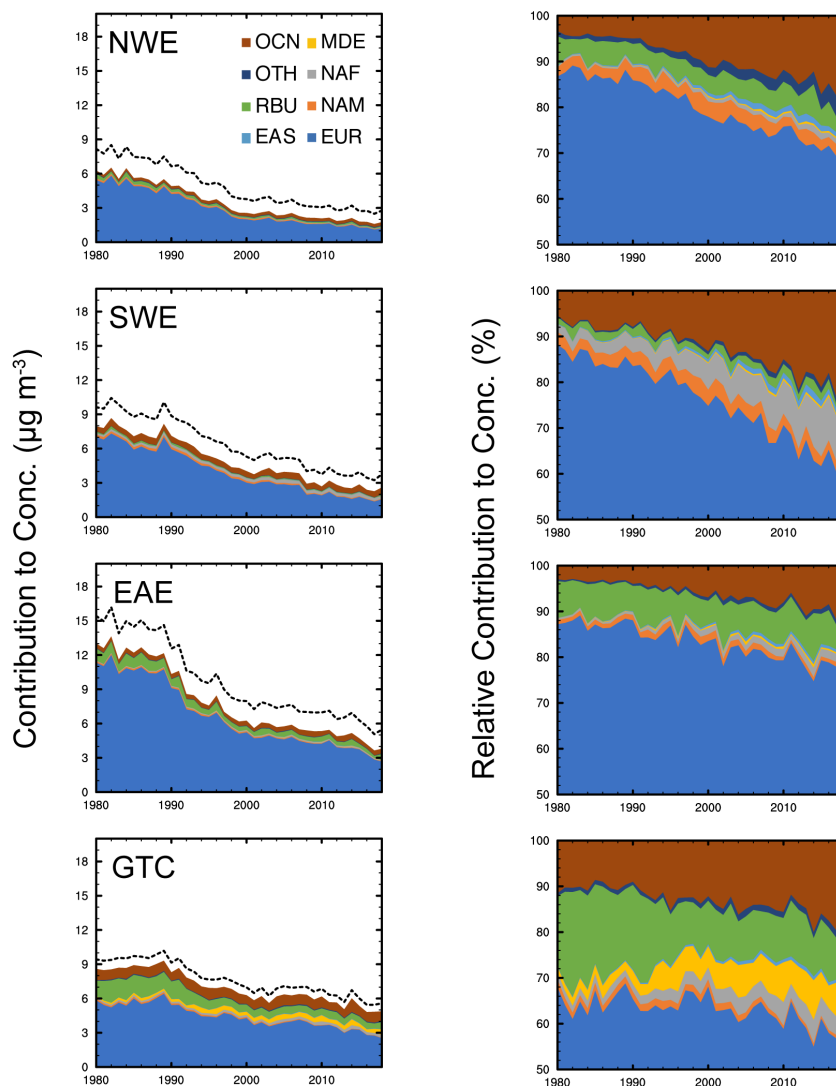
712
713
714
715
716
717
718

Figure 5. (a,b) Absolute ($\mu\text{g m}^{-3}$) and (c,d) relative contributions (%) to annual mean near-surface concentrations of sulfate-BC-POA from European local emissions and emissions outside the Europe, respectively, averaged over 2010–2018.



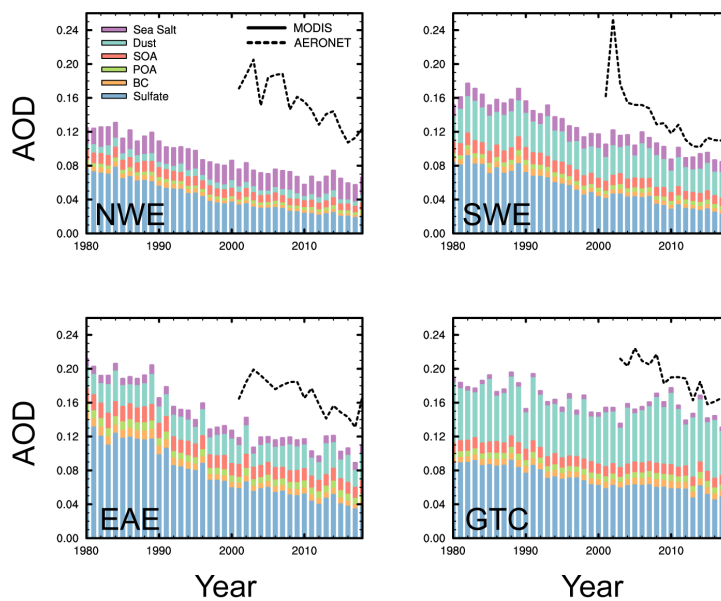
719
720
721
722
723
724
725
726
727
728
729

Figure 6. Relative contributions (%) by emissions from major tagged source regions (EUR, NAM, NAF, MDE, EAS, RBU, OCN) and other regions (OTH=CAM+SAM+SAF+SEA+CAS+SAS+PAN+ARC+ANT) to near-surface concentrations (left) and column burdens (right) of sulfate, BC and POA (from top to bottom) in the four sub-regions of Europe averaged over 2010–2018. Patterned areas represent EUR local contributions.



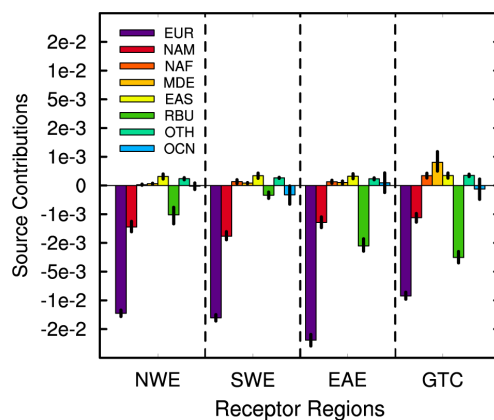
730
731
732
733
734
735
736
737
738

Figure 7. Time series (1980–2018) of absolute (left, $\mu\text{g m}^{-3}$) and relative (right, %) contributions of emissions from major source regions to the simulated annual mean near-surface sulfate-BC-POA concentrations averaged over the four sub-regions of Europe. Dashed lines in left panels represent simulated aerosol concentrations including SOA.



739
740
741
742
743
744
745

Figure 8. Time series (1980–2018) of simulated annual mean AOD for sulfate, BC, POA, SOA, dust and sea salt averaged over the four sub-regions of Europe. Dashed lines represent AOD from AERONET measurements.



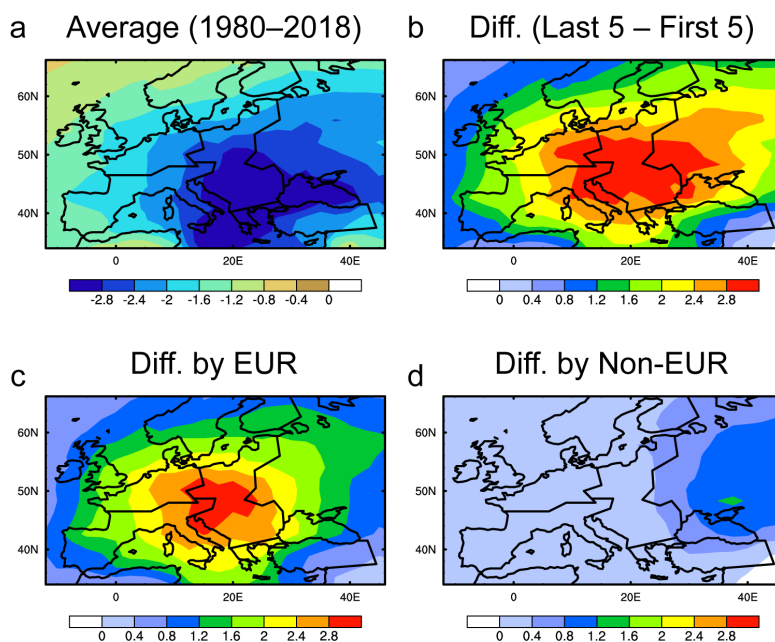
746

747

748 **Figure 9.** Absolute contributions (decade^{-1}) of the emissions from major source
749 regions to the trends of sulfate AOD over the four sub-regions of Europe. Error bars
750 represent 95% confidence intervals of the linear regression.

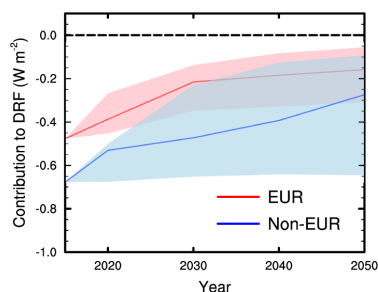
751

752



753
754
755
756
757
758
759

Figure 10. (a) Simulated annual mean DRF (W m^{-2}) of sulfate averaged over 1980–2018 and (b) the difference in sulfate DRF between 1980–1984 and 2014–2018. The contributions of European and non-European emissions to the difference are given in (c) and (d), respectively.



760

761

762 **Figure 11.** Time series (2015–2050) of estimated annual mean sulfate DRF over
763 Europe contributed by European and non-European emissions. Lines and areas
764 represent median values and minimum-to-maximum ranges of the estimated sulfate
765 DRF from eight SSP scenarios, including SSP1-1.9, SSP1-2.6, SSP2-4.5, SSP3-7.0,
766 SSP4-3.4, SSP4-6.0, SSP5-3.4, and SSP5-8.5. Future DRF of sulfate aerosol over
767 Europe is estimated by scaling historical mean (1980–2018) sulfate DRF using the
768 ratio of SSPs future SO₂ emissions to historical emissions assuming a linear
769 response of DRF to regional emissions.

770